▌ **Synthesis Design**

Construction of Large-Area Uniform Graphdiyne Film for High-Performance Lithium-Ion Batteries

Jianjiang He,[a] Kaijing Bao,[b] Weiwei Cui,[c] Jiaojiao Yu,[a] Changshui Huang,*[a] Xiangyan Shen,[a] Zili Cui,[a] and Ning Wang[a]

Abstract: Large-area graphdiyne film is constructed by heat treatment, including thermally induced evaporation and a cross-coupling reaction process. The growth mechanism is proposed based on the observation and characterization that the heating temperature plays an important role in the evaporation of oligomers and in triggering the thermal cross-coupling reaction, whereas the heating duration mainly determines the execution of the thermal cross-coupling reaction. By controlling the heat-treatment process, a graphdiyne film with uniform morphology and good con-ductivity is obtained. The improved GDY film based electrodes deliver good interfacial contact and more lithium storage sites; thus leading to superior electrochemical performance. A reversible capacity of 901 mAh g^{-1} is achieved. Specifically, the electrodes exhibit excellent rate performance, with which a capacity of 430 mAh g^{-1} is maintained at a rate as high as 5 A g^{-1}. These advantages mean that the uniform graphdiyne film is a good candidate for the fabrication of a flexible and high-capacity electrode material.

Introduction

Graphdiyne (GDY), as a new 2D carbon allotrope with sp^2- and sp-hybridized carbon atoms, has received tremendous attention due to its high performance in many applications, such as photocatalysis,[1] electrocatalysis,[2] solar cells,[3] oil/water separation,[4] supercapacitors,[5] and lithium-ion batteries (LIBs).[6] This unique atomic structure endows GDY with a π-conjugated 2D layer plane, uniformly distributed pores, and good conductivity, which play important roles in electrochemical performance.[7] Many theoretical calculations have predicted the high capacity and good rate performance of GDY as a very promising anode material for LIBs. The theoretical capacity of monolayered GDY is 744 mAh g^{-1}, whereas that of multilayered GDY is more than 1000 mAh g^{-1}.[8] The actual reversible capacity of GDY film reaches only 612 mAh g^{-1} at a current density of 100 mA g^{-1} in a practical LIB, which is lower than that predicted.[6] This motived us to seek improvements for applying GDY in electrode materials.

It is reported that the good interfacial compatibility between the bulk electrode material and electrolyte is beneficial for good electrochemical performance.[9] The construction of GDY with uniform morphology and interface compatibility is meaningful for the application of GDY in LIBs.[10] Because the synthesis of GDY is mainly achieved through a Glaser coupling reaction, considering that GDY is a 2D planar structure, the fast chemical reaction will also result in some small-molecule pieces of GDY, such as its oligomers, as well as defects and some amorphous phase, which may affect the quality of GDY, its interface compatibility, and electrochemical performance. It is reported that the structural development of carbon materials during heat treatment is a thermally activated kinetic process.[9, 11] Kim et al. reported that a high-purity carbon nanofiber web, which was thermally treated at 2800 °C in an inert atmosphere, displayed a morphological transformation from a smooth to a wrinkled surface.[9] Wang et al. introduced uniform graphene nanosheets prepared by a rapid heating process and subsequent ultrasonic treatment.[11c] For us, heat treatment, including the annealing method, may pave the way to improving the quality of film and bulk GDY because heat treatment may remove oligomers, provide conditions for self-repairing the defects and flaws of GDY, and improve the interfacial compatibility of GDY.

Herein, we report on the construction of large-area uniform GDY films through heat treatment. SEM and TEM images of GDY films reveal the uniform morphology and demonstrate the evolution process. The UV/Vis absorption spectrum and I–V curves suggest the preparation of GDY films with good conductivity after the cross-coupling reaction. Benefitting from the uniform interface and good conductivity, the GDY film exhibits a highly improved reversible capacity of 901 mAh g^{-1} for LIBs

[a] Dr. J. He, J. Yu, Prof. C. Huang, X. Shen, Dr. Z. Cui, Dr. N. Wang
Qingdao Institute of Bioenergy and Bioprocess Technology
Chinese Academy of Sciences, No. 189 Songling Road
Qingdao 266101 (P.R. China)
E-mail: huangcs@qibebt.ac.cn

[b] K. Bao
Qingdao University of Science and Technology
No. 53 Zhengzhou Road, Qingdao 266042 (P.R. China)

[c] W. Cui
Qingdao University, No. 308 Ningxia Road, Qingdao
266071 (P.R. China)

🖳 Supporting information and the ORCID identification numbers for the authors of this article can be found under https://doi.org/10.1002/chem.201704581.

at a current density of $100\,mA\,g^{-1}$. Remarkably, this uniform film still maintains a capacity of $430\,mAh\,g^{-1}$ at a rate as high as $5\,A\,g^{-1}$.

Results and Discussion

Morphological and structural evolution of GDY films

We performed heat treatment on fabricated GDY at different temperatures for different time periods (Figure S1 in the Supporting Information). It is observed in the thermogravimetric (TG) profile that the fabricated GDY manifests continuous weight loss until 600 °C, which suggests the existence of oligomers (Figure S2 in the Supporting Information). The heat-treatment process and results were observed by SEM. The SEM images show that there are many GDY nanoparticles, which are about 700 nm in diameter, on the surface of GDY film after calcination at 200 °C for 2 h (Figure 1 a). Magnification shows that the film is composed of melted nanoparticles. It can be seen from Figure 1 b that some of the nanoparticles are eliminated during calcination at 300 °C for 2 h. Meanwhile, the jagged and porous surface shown in Figure 1 b reveals that many embedded oligomers and particles with a low gasification temperature in the bulk of the GDY films evaporate under heat treatment. These results indicate that the evolution of GDY films is dominated by an evaporation process at a heating temperature of 200 and 300 °C. As the heating temperature increased to 400 °C, most nanoparticles were removed from the surface to construct uniform and smooth GDY films (Fig-

ure 1 c). This process may be attributed to both evaporation of oligomers and some self-repair process, in which the cross-coupling reaction takes place on small pieces and defects of the GDY film surface.[12] The proposed growth mechanism of the uniform film is illustrated in Figure 1 e. The GDY nanoparticles either take part in the cross-coupling reaction or evaporate with the increasing heating temperature, which smooths the surface of GDY. However, uniform films are broken and many GDY nanospheres, with a diameter of 60 nm, emerge at a heating temperature of 500 °C (Figure 1 d). This phenomenon can be explained because the morphology of generated GDY is prone to form spheres, rather than films, to reduce the surface energy at high temperatures.[13]

The evolution of the GDY morphology at different temperatures can also be observed in the TEM images in Figure 2 a–d. Stacked layers are observed in all samples, which suggests the 2D structure of GDY films. The GDY particles are distinguishable in the TEM images in Figure 2 a–d, which is consistent with the results in SEM images (Figure 1 a–d). Figure 2 a shows the sample treated at 200 °C. The GDY film was compact without clear pores, whereas at 300 °C the GDY film revealed a porous structure (Figure 2 b), which confirmed evaporation of the GDY oligomers. At 400 °C (Figure 2 c), the porous structure is clearer than that in Figure 2 b; this indicates that many GDY oligomers have evaporated, which would benefit a high surface area. This porous structure is not observed in the SEM images (Figure 1 c), which suggests that the self-repair reaction preferentially occurs at the surface, rather than in the bulk, because of sufficient evaporation of oligomers from the surface. The porous structure decreased to a small piece of the GDY film if the temperature was raised to 500 °C (Figure 2 d). This phenomenon can be ascribed to the broken bulk film, and consequently, facilitation of the self-repair reaction in more regions.

The chemical structure was characterized by XPS (Figure 2 e–h and Figure S3 in the Supporting Information). It is observed in Figure 2 e–h that there is no significant change between any of the samples treated at different temperatures, or those that
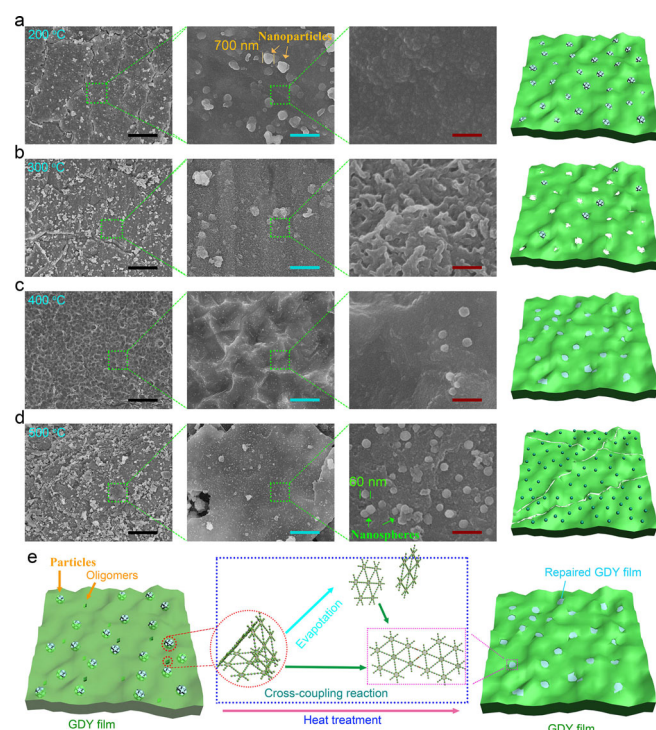
Figure 1. SEM images of GDY heated at different temperatures: a) heated at 200 °C for 2 h, b) heated at 300 °C for 2 h, c) heated at 400 °C for 2 h, and d) heated at 500 °C for 2 h. Scale bars: 20 μm (black), 2 μm (green), 200 nm (red). e) The proposed growth mechanism of uniform GDY film.
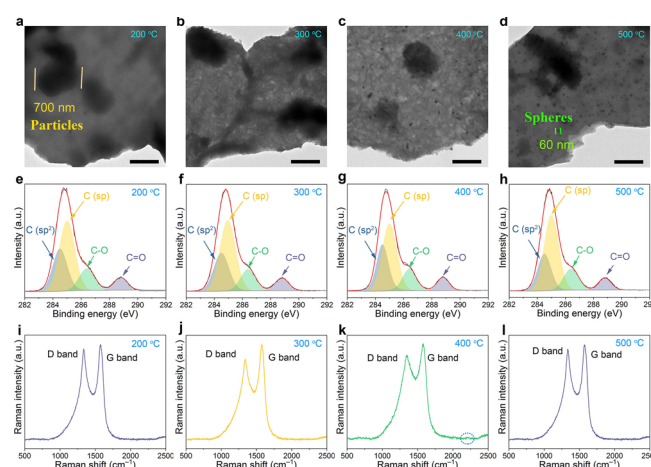
Figure 2. TEM images (a–d), X-ray photoelectron spectroscopy (XPS) results (e–h), and Raman spectra (i–l) of heat-treated GDY at different temperatures: a) treated at 200 °C for 2 h, b) treated at 300 °C for 2 h, c) treated at 400 °C for 2 h, and d) treated at 500 °C for 2 h. Scale bars: 500 nm.

↖↖ **These are not the final page numbers!**

are untreated, which implies that the main structure of the samples does not change after heat treatment under argon (Figure S4a in the Supporting Information). In detail, the C 1s peaks of GDY in Figure 2e–h can be deconvoluted into four subpeaks of C—C (sp^2) at 284.5 eV, C—C (sp) at 285 eV, C—O at 286.4 eV, and C=O at 288.8 eV. XPS data shows that the synthetic products have both sp^2- and sp-hybridized carbon, and the area ratio of the two is close to 1:2, which is consistent with the reported structure.[14] In the fitting peaks of carbon, we have also found a lot of oxygen, which may be because GDY has a high specific surface area and a large number of pores, and thus, has a strong adsorption ability for O_2 upon exposure to air. Figure 2i–l shows that the Raman spectra of the as-synthesized samples exhibit two main bands. A G band at 1584 cm^{-1} suggests that the products possess abundant aromatic rings, and a D band at 1356 cm^{-1} corresponds to defects and edges.[15] It can be observed that the intensity of the D band decreases due to the self-repair reaction. The inconspicuous band at 2200 cm^{-1} can be observed in Figure 2k, which is assigned to the acetylenic bond. The increasing intensity of the D band, in comparison with that of untreated GDY, may be due to defects generated at 200 °C (Figure S4b in the Supporting Information).

UV/Vis absorption spectroscopy was used to characterize the electronic conductivity of GDY films (Figure S5 in the Supporting Information). The energy gaps between the HOMO and LUMO of the heat-treatment samples were measured to be 1.31 eV for the untreated sample, 1.52 eV for that treated at 200 °C, 1.22 eV for that treated at 300 °C, 1.02 eV for that treated at 400 °C, and 0.94 eV for that treated at 500 °C (Figure 3a).[16] The I–V curves indicate that the conductivity is 2.26×10^{-4}, 1.86×10^{-5}, 6.07×10^{-4}, 2.56×10^{-3}, and 6.45×10^{-3} S m^{-1} for the untreated sample and those heated at 200, 300, 400, and 500 °C, respectively (Figure 3b). The decreasing energy gap and increasing conductivity with increasing treatment temperature reveals the improved quality of the GDY film; this can be ascribed to the elimination and possible self-repair cross-coupling process of GDY oligomers and pieces. The slight reduction in conductivity, in comparison with that of untreated GDY, may be ascribed to defects generated upon the evaporation of oligomers at a heating temperature of 200 °C.

The influence of heat-treatment duration on the synthesis of GDY has also been investigated (Figure S6 in the Supporting Information). Particles exist on the surface until GDY has been heated for as long as 2 h at 400 °C. The formation of the smooth GDY film is clearly observed in Figure S6b and e in the Supporting Information; thus the self-repair reaction has occurred. Although the surface of the GDY film becomes smooth, some oligomers exist on it due to the short heating duration (Figure S6a and d in the Supporting Information). The SEM images in Figure S6a, d, and g in the Supporting Information demonstrate that the self-repair process is limited by the duration of the cross-coupling reaction and evaporation of oligomers over 2 h. However, uniform GDY spheres emerged as the heating time is prolonged to 3 h, which suggests the instability of the newly formed GDY film morphology over a long heating duration at high temperature (Figure S6j–l in the Supporting Information). As far as the roles of heating temperature and duration in the formation of uniform GDY film are concerned, it can be concluded that a heating temperature of 400 °C is beneficial for both evaporation and further cross-coupling reaction of oligomers for a heating time of 2 h to ensure that the self-repair of the GDY film can proceed properly.

The time-dependent GDY film self-repair process at 400 °C can be clearly observed in the TEM images shown in Figure S7a–d in the Supporting Information. The porous structure can be clearly observed in the samples treated for 0.5, 1, and 2 h. This phenomenon demonstrates that the evaporation of oligomers takes place in the bulk film. The evolution of the particles is clearly realized. There are many particles on the surface of the formed uniform film heated for 0.5 and 1 h (Figure S7a and b in the Supporting Information). These particles are eliminated as heating continues for 2 h (Figure S7c in the Supporting Information). Nevertheless, GDY spheres emerge because they are energetically favorable as the heating duration is prolonged to 3 h (Figure S7d in the Supporting Information). XPS spectra demonstrate that the position of the four subpeaks and the area ratio of sp^2- and sp-hybridized carbon does not change for different heating durations, which suggests that the chemical structure does not evolve during the heat-treatment process (Figures S7e and S8 in the Supporting Information). As shown in Figure S7f in the Supporting Information, Raman spectra also reveal a comparable intensity between D and G bands in all samples. The result is consistent with that at different temperatures, which reveals a stable chemical structure throughout the heating process. The energy gaps of the samples heated for different times were calculated by the transformation of UV/Vis absorption spectra (Figures S7g and S9 in the Supporting Information). The energy gaps of the samples evolved from 1.16, 1.11, 1.02 to 0.96 eV as the samples were heated for 0.5, 1, 2, and 3 h, respectively, at 400 °C. The I–V curves in Figure S7h in the Sup-
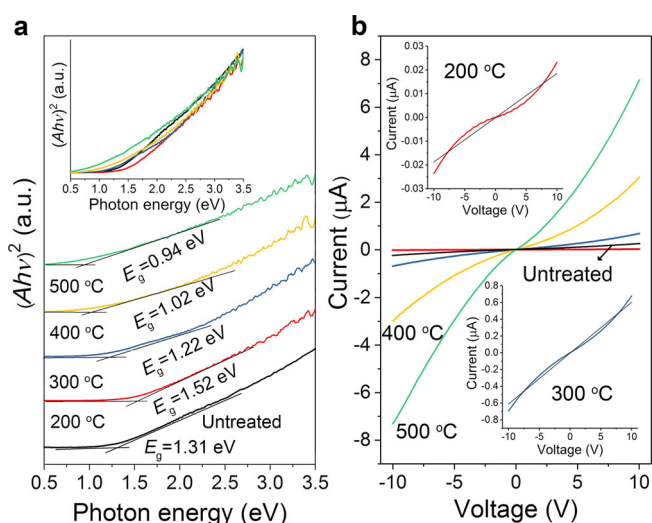
Figure 3. a) Transformation of the UV/Vis spectrum for heat-treated GDY; inset: plots of $(Ah\nu)^2$ versus photon energy ($h\nu$). b) I–V curves of heat-treated GDY.

These are not the final page numbers! ↗↗

porting Information show that the conductivity of the samples is calculated to be 8.93×10^{-4}, 1.19×10^{-3}, 2.56×10^{-3}, and $4.84 \times 10^{-3} \, S\,m^{-1}$ for the samples heated 0.5, 1, 2, and 3 h at 400 °C. The similar values of conductivities indicate the occurrence of similar self-repair reactions, regardless of heating duration. These results demonstrate that the heating duration plays an important role in the further execution of the thermal cross-coupling reaction of GDY oligomers and pieces.

Electrochemical performance of GDY films

The electrochemical performances of the GDY film electrodes were evaluated by using half-cells with lithium metal as a reference electrode over the potential range of 0.005–3 V versus Li^+/Li. Figure 4a–d shows the rate performance of electrodes composed of the GDY film treated at different temperatures from 0.1 to 5 Ag^{-1}. All electrodes, except the sample heated at 500 °C, can recover from the high current density and show a decent rate performance. It can be clearly observed that the reversible capacity is different at a current density of 100 $mA\,g^{-1}$ for different heating temperatures (Figure 4a–d). The initial Coulombic efficiency (CE) of the electrodes is 58.8, 44.0, 44.7, and 50.8% for the samples heated at 200, 300, 400, and 500 °C, respectively. The reversible capacity increases with increasing heating temperature from 200 to 400 °C because of the increasing conductivity. The lower reversible capacity of samples heated at 200 and 300 °C is ascribed to the existence of oligomers and particles, which exhibit a low conductivity,

and thus, limited active binding sites.[17] However, the reversible capacity starts to reduce as the heating temperature rises to 500 °C. This phenomenon may be ascribed to poor diffusion of lithium ions through the newly generated GDY spheres and compact sheets, in spite of better conductivity at 500 °C. It can be seen from Figure S10 in the Supporting Information that the Galvanostatic charge/discharge curves of samples heated for 2 h at different temperatures are similar to each other; this indicates that there are no clear redox peaks, which is consistent with previous work.[6] Figure 4e shows the cyclic stabilities of different samples. The samples show good cycle performance, except for the one heated at 500 °C. The reversible capacity can reach 272, 689, 901, and 578 $mAh\,g^{-1}$ for heat-treated samples at 200, 300, 400, and 500 °C after 150 cycles at a current density of 100 $mA\,g^{-1}$. The low reversible capacity of the free-standing film treated at 200 °C is due to the lack of conductivity or current collectors, in comparison with the reported untreated GDY.[6]

The CE of the sample heated at 400 °C is about 98.2%, on average. The different cycle performance between the samples heated at 400 and 500 °C suggests that the uniform film is beneficial for good electrochemical stability, which is dominated by the interfacial reaction. The reversible capacity of GDY heated at 400 °C is higher than that of most carbon materials, including GDY on copper foil, natural graphite (NG), carbon nanotubes (CNTs), graphene, and comparable to that of N-doped porous carbon nanofibers (N-CNFs) and hollow CNTs/CNFs in LIBs (Table 1). Although a much higher capacity is obtained for N-doped porous carbon, it always suffers from instability due to the high amount of defects. In addition, GDY films treated at different temperatures exhibit superior cyclic stability to that of graphene sheets, which contain abundant edges due to the synthetic route.[11c]

Interfacial charge transfer and the lithium-ion diffusion process in the electrode were characterized by SEM and electrochemical impedance spectroscopy (EIS). Figure 5a–d shows the SEM images of the formed solid–electrolyte interface (SEI) film
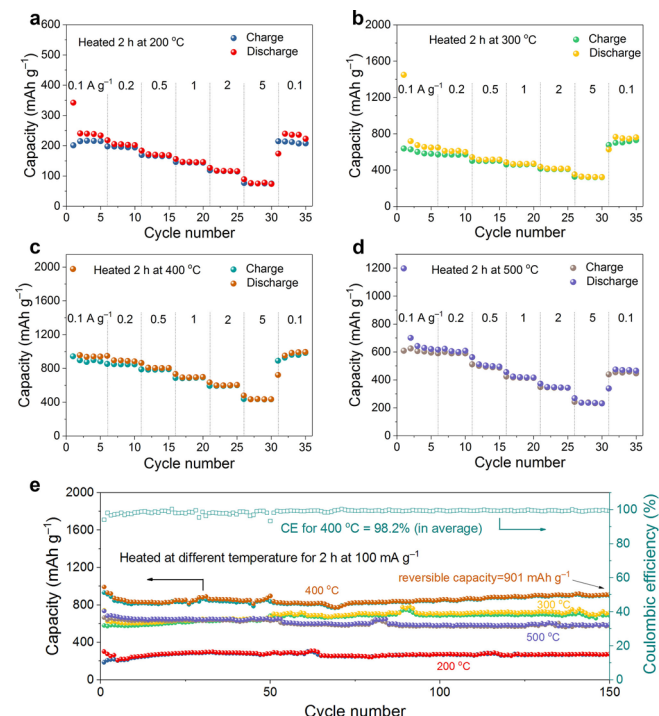
Figure 4. The rate performance of heat-treated GDY at different temperatures: a) treated at 200 °C for 2 h, b) treated at 300 °C for 2 h, c) treated at 400 °C for 2 h, and d) treated at 500 °C for 2 h. e) The cycling performance of heat-treated GDY at different temperatures; the current density is 100 $mA\,g^{-1}$.

Table 1. Reversible capacities of carbon materials as anodes in LIBs.

Electrode	Reversible capacity [$mAh\,g^{-1}$]	Discharge rate	Ref.
GDY film	901	100 $mA\,g^{-1}$	this work
GDY film	807	500 $mA\,g^{-1}$	this work
GDY on Cu	612	100 $mA\,g^{-1}$	[6]
NG	360	15 $mA\,g^{-1}$	[18]
CNT	200	400 $mA\,g^{-1}$	[19]
hard carbon	424	30 $mA\,g^{-1}$	[20]
graphene	460	1 C	[11c]
N-graphene	872	50 $mA\,g^{-1}$	[21]
B-graphene	700	500 $mA\,g^{-1}$	[21]
3D graphene	659	0.5 C	[22]
N-CNTs	516	200 $mA\,g^{-1}$	[23]
N-CNFs	1280	100 $mA\,g^{-1}$	[24]
N-CNFs	924	500 $mA\,g^{-1}$	[24]
hollow CNTs/CNFs	1150	100 $mA\,g^{-1}$	[25]
N-doped porous carbon	2132	100 $mA\,g^{-1}$	[26]
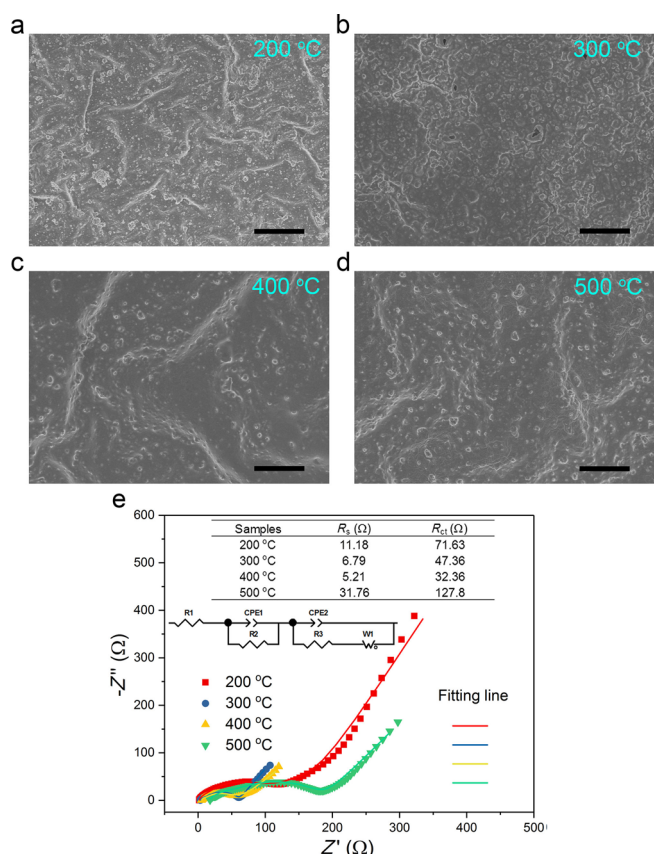
Figure 5. SEM images of heat-treated GDY at different temperatures for LIBs after cycling: a) treated at 200 °C for 2 h, b) treated at 300 °C for 2 h, c) treated at 400 °C for 2 h, and d) treated at 500 °C for 2 h. Scale bars: 20 μm. e) EIS of the electrodes after cycling; inset shows the equivalent circuit and fitting parameters. CPE = constant-phase element.

on samples heated at different temperatures. The SEI film of the sample heated at 400 °C is more uniform than that of the others. High-resolution TEM was performed on GDY films heated at 300 and 400 °C before and after lithium intercalation; these results demonstrated changes in the layer distance. It can be observed from Figure S11 in the Supporting Information that the layer distance of heated GDY films is about 0.365 nm, which is consistent with untreated GDY. Furthermore, the layer ordering is almost maintained after cycling. This good interfacial compatibility can also be observed in the EIS results. The equivalent circuit model of the studied system can be observed in Figure 5e. The indistinct semicircle in the high-frequency region corresponds to the SEI film resistance (R_s) and the constant-phase element (CPE1), the medium-frequency semicircle is assigned to the charge-transfer impedance (R_{ct}) and the CPE of the electrode–electrolyte interface (CPE2), and W in the low-frequency region is associated with the Warburg impedance.[27] The fitting parameters are listed in the inset of Figure 5e. The low R_s and R_{ct} values of the sample heated at 400 °C suggest good interface contact between the uniform GDY film and SEI film, which would minimize side reactions.

Figure S12 in the Supporting Information shows the electrochemical performance of the as-synthesized samples heated

for different times. The rate performance of the samples treated at 400 °C for different times is similar to that of samples treated at different temperatures. However, the samples heated at 400 °C exhibited superior reversible capacity than that of the sample heated at 200 °C due to good conductivity. The sample heated for 0.5 h at 400 °C shows a lower capacity than that of the others; this can be ascribed to the existence of numerous oligomers. The extremely similar electrochemical behavior between the samples heated for 1 and 2 h at 400 °C contributes to the similar morphology and interfacial contact (Figure S6 in the Supporting Information). The sample heated for 3 h delivers rapid degradation of capacity because of the GDY spheres; this is consistent with the results observed in Figure 4d. Galvanostatic charge/discharge curves of samples heated for different times are shown in Figure S13 in the Supporting Information and reveal the analogical electrochemical process in these samples. The cycle performance of the samples heated at 400 °C for different times is depicted in Figure S12e in the Supporting Information. Reversible capacities of 257, 658, 807, and 345 mAh g^{-1} are achieved for samples treated at 400 °C for 0.5, 1, 2, and 3 h at a current density of 500 mA g^{-1} after 300 cycles. Excellent cycling stability can be observed for the electrochemical performance of samples heated for 0.5, 1, and 2 h. Specifically, the CE of the sample heated at 400 °C for 2 h is as high as 99.8 %.

It can be observed from Figure S14 a–d in the Supporting Information that GDY particles or spheres influence the formation of a uniform SEI film. Broken films in Figure S14 a and d in the Supporting Information suggest an unstable interface, as characterized by EIS. Figure S14 e in the Supporting Information shows Nyquist plots of samples heated for different times at 400 °C; the equivalent circuit and fitting parameters are also listed. Samples heated for 0.5 and 3 h at 400 °C have a large interfacial resistance due to the existence of GDY particles and spheres. The low resistance and uniform morphology of the SEI film for both samples heated for 1 and 2 h are beneficial for the reduction of the interfacial reaction, which results in a superior rate performance and cycling stability.

Conclusion

Improved uniform GDY film was prepared by a thermal method. SEM and TEM images revealed that the heating temperature played important roles in both the evaporation of oligomers and triggering of the thermal cross-coupling reaction, whereas the heating duration mainly determined execution of the thermal cross-coupling reaction. Through the optimization of both factors, large-area uniform GDY film was obtained that demonstrated good interface contact, as evidenced by SEM images after cycling and EIS. Furthermore, good conductivity was achieved through the cross-coupling of oligomers. These advantages endow the improved uniform GDY film with excellent electrochemical behavior, including large reversible capacity, good rate, and stable cycling performance.

Experimental Section

Synthesis

GDY films were obtained through the synthetic route described in ref. [6] followed by heat treatment under an argon atmosphere (Figure 1). The heating temperature was from 200 to 500 °C and heating was maintained at the required temperature for 2 h. Furthermore, samples were heated for different times at 400 °C. The heating rate was 5 °C min^{-1} and samples were cooled to room temperature spontaneously. A detailed synthetic method is given in the Supporting Information.

Characterization

Morphology details were examined by means of field-emission SEM (HITACHI S-4800) and TEM (HITACHI H-7650). The chemical structure of the samples was characterized by Raman spectroscopy (Thermo Scientific DXRxi, 532 nm). XPS results were collected on a VG Scientific ESCALab220i-XL X-ray photoelectron spectrometer, with Al$_{K\alpha}$ radiation as the excitation source. UV/Vis adsorption spectroscopy was recorded on a HITACHI U-4100 spectrometer. The *I–V* curves were measured on a Keithley 4200 SCS instrument. A Rubotherm DynTHERM instrument was used to perform TG analysis.

Electrochemical analysis

Electrochemical measurements were performed by using CR2032 coin-type cells assembled in an argon-filled glovebox. The half-cells were assembled by using the GDY films as the cathode, Li metal foil as the anode, a polypropylene separator (Celgard 2500), and a liquid electrolyte (ethylene carbonate/dimethyl carbonate, 1:1 v/v) containing 1.0 M LiPF$_6$ for LIBs were used. The assembled half-cells were cycled between 0.005 and 3 V by using a LAND battery testing system. EIS measurements were carried out on a CHI760 electrochemical work station from CH Instruments by applying an alternating current (AC) voltage with an amplitude of 5 mV at room temperature.

Conflict of interest

The authors declare no conflict of interest.

[1] a) J. Li, X. Gao, B. Liu, Q. Feng, X. B. Li, M. Y. Huang, Z. Liu, J. Zhang, C. H. Tung, L. Z. Wu, *J. Am. Chem. Soc.* **2016**, *138*, 3954; b) S. Wang, L. Yi, J. E. Halpert, X. Lai, Y. Liu, H. Cao, R. Yu, D. Wang, Y. Li, *Small* **2012**, *8*, 265; c) N. Yang, Y. Liu, H. Wen, Z. Tang, H. Zhao, Y. Li, D. Wang, *ACS Nano* **2013**, *7*, 1504; d) X. Gao, J. Li, R. Du, J. Zhou, M. Y. Huang, R. Liu, J. Li, Z. Xie, L. Z. Wu, Z. Liu, *Adv. Mater.* **2016**, *28*, 1605308.

[2] a) R. Liu, H. Liu, Y. Li, Y. Yi, X. Shang, S. Zhang, X. Yu, S. Zhang, H. Cao, G. Zhang, *Nanoscale* **2014**, *6*, 11336; b) H. Qi, P. Yu, Y. Wang, G. Han, H. Liu, Y. Yi, Y. Li, L. Mao, *J. Am. Chem. Soc.* **2015**, *137*, 5260.

[3] a) J. Xiao, J. Shi, H. Liu, Y. Xu, S. Lv, Y. Luo, D. Li, Q. Meng, Y. Li, *Adv. Energy Mater.* **2015**, *5*, 1401943; b) H. Ren, H. Shao, L. Zhang, D. Guo, Q. Jin, R. Yu, L. Wang, Y. Li, Y. Wang, H. Zhao, D. Wang, *Adv. Energy Mater.* **2015**, *5*, 1500296; c) C. Kuang, G. Tang, T. Jiu, H. Yang, H. Liu, B. Li, W. Luo, X. Li, W. Zhang, F. Lu, J. Fang, Y. Li, *Nano Lett.* **2015**, *15*, 2756.

[4] X. Gao, J. Zhou, R. Du, Z. Xie, S. Deng, R. Liu, Z. Liu, J. Zhang, *Adv. Mater.* **2016**, *28*, 168.

[5] H. Du, H. Yang, C. Huang, J. He, H. Liu, Y. Li, *Nano Energy* **2016**, *22*, 615.

[6] C. Huang, S. Zhang, H. Liu, Y. Li, G. Cui, Y. Li, *Nano Energy* **2015**, *11*, 481.

[7] a) S. Zhang, J. He, J. Zheng, C. Huang, Q. Lv, K. Wang, N. Wang, Z. Lan, *J. Mater. Chem. A* **2017**, *5*, 2045; b) S. Zhang, H. Liu, C. Huang, G. Cui, Y. Li, *Chem. Commun.* **2015**, *51*, 1834; c) S. Zhang, J. He, C. Huang, H. Liu, G. Cui, Y. Li, *ACS Appl. Mater. Interfaces* **2016**, *8*, 8467.

[8] a) C. Sun, D. J. Searles, *J. Phys. Chem. C* **2012**, *116*, 26222; b) H. J. Hwang, J. Koo, M. Park, N. Park, Y. Kwon, H. Lee, *J. Phys. Chem. C* **2013**, *117*, 6919.

[9] C. Kim, K. S. Yang, M. Kojima, K. Yoshida, Y. J. Kim, Y. A. Kim, M. Endo, *Adv. Funct. Mater.* **2006**, *16*, 2393.

[10] R. Raccichini, A. Varzi, S. Passerini, B. Scrosati, *Nat. Mater.* **2015**, *14*, 271.

[11] a) P. A. Thrower, *Chemistry and Physics of Carbon*, CRC, Boca Raton, **1996**; b) P. Guo, H. Song, X. Chen, *Electrochem. Commun.* **2009**, *11*, 1320; c) G. Wang, X. Shen, J. Yao, J. Park, *Carbon* **2009**, *47*, 2049.

[12] a) X. Qian, Z. Ning, Y. Li, H. Liu, C. Ouyang, Q. Chen, Y. Li, *Dalton Trans.* **2012**, *41*, 730; b) X. Qian, H. Liu, C. Huang, S. Chen, L. Zhang, Y. Li, J. Wang, Y. Li, *Sci. Rep.* **2015**, *5*, 7756; c) J. Zhou, X. Gao, R. Liu, Z. Xie, J. Yang, S. Zhang, G. Zhang, H. Liu, Y. Li, J. Zhang, Z. Liu, *J. Am. Chem. Soc.* **2015**, *137*, 7596.

[13] a) L. Xiao, J. Damien, J. Luo, H. D. Jang, J. Huang, Z. He, *J. Power Sources* **2012**, *208*, 187; b) J. He, C. Niu, C. Yang, J. Wang, X. Su, *RSC Adv.* **2014**, *4*, 60253.

[14] G. Li, Y. Li, H. Liu, Y. Guo, Y. Li, D. Zhu, *Chem. Commun.* **2010**, *46*, 3256.

[15] a) S. Zhang, J. Wang, Z. Li, R. Zhao, L. Tong, Z. Liu, J. Zhang, Z. Liu, *J. Phys. Chem. C* **2016**, *120*, 10605; b) J. Wang, S. Zhang, J. Zhou, R. Liu, R. Du, H. Xu, Z. Liu, J. Zhang, Z. Liu, *Phys. Chem. Chem. Phys.* **2014**, *16*, 11303; c) A. C. Ferrari, D. M. Basko, *Nat. Nanotechnol.* **2013**, *8*, 235.

[16] T. Yu, B. Lim, Y. Xia, *Angew. Chem. Int. Ed.* **2010**, *49*, 4484; *Angew. Chem.* **2010**, *122*, 4586.

[17] a) J. Liu, K. Song, C. Zhu, C.-C. Chen, P. A. van Aken, J. Maier, Y. Yu, *ACS Nano* **2014**, *8*, 7051; b) B. Wang, X. Li, X. Zhang, B. Luo, M. Jin, M. Liang, S. A. Dayeh, S. T. Picraux, L. Zhi, *ACS Nano* **2013**, *7*, 1437.

[18] H. Zheng, K. Jiang, T. Abe, Z. Ogumi, *Carbon* **2006**, *44*, 203 – 210.

[19] S. W. Lee, N. Yabuuchi, B. M. Gallant, S. Chen, B.-S. Kim, P. T. Hammond, Y. Shao-Horn, *Nat. Nanotechnol.* **2010**, *5*, 531 – 537.

[20] Y.-J. Han, D. Chung, K. Nakabayashi, J.-D. Chung, J. Miyawaki, S.-H. Yoon, *Electrochim. Acta* **2016**, *213*, 432 – 438.

[21] Z.-S. Wu, W. Ren, L. Xu, F. Li, H.-M. Cheng, *ACS Nano* **2011**, *5*, 5463 – 5471.

[22] J. Tang, G. Chen, J. Yang, X. Zhou, L. Zhou, B. Huang, *Nano Energy* **2014**, *8*, 62 – 70.

[23] Z. Pan, J. Ren, G. Guan, X. Fang, B. Wang, S. G. Doo, I. H. Son, X. Huang, H. Peng, *Adv. Energy Mater.* **2016**, *6*, 1600271.

[24] L. Qie, W. M. Chen, Z. H. Wang, Q. G. Shao, X. Li, L. X. Yuan, X. L. Hu, W. X. Zhang, Y. H. Huang, *Adv. Mater.* **2012**, *24*, 2047 – 2050.

[25] Y. Chen, X. Li, K. Park, J. Song, J. Hong, L. Zhou, Y.-W. Mai, H. Huang, J. B. Goodenough, *J. Am. Chem. Soc.* **2013**, *135*, 16280 – 16283.

[26] F. Zheng, Y. Yang, Q. Chen, *Nat. Commun.* **2014**, *5*, 5261.

[27] J. He, C. Zhang, H. Du, S. Zhang, P. Hu, Z. Zhang, Y. Ma, C. Huang, G. Cui, *Electrochim. Acta* **2015**, *178*, 476 – 483.

↖↖ These are not the final page numbers!
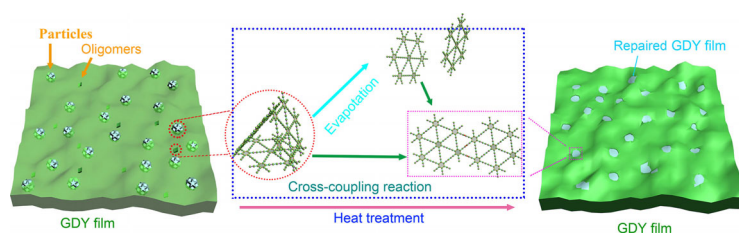
Turn up the heat! A large-area uniform graphdiyne (GDY) film has been constructed through thermal treatment for application in high reversible capacity lithium-ion batteries (see figure). The heating temperature plays an important role in the evaporation of oligomers and in triggering the thermal cross-coupling reaction, whereas the heating duration mainly determines the execution of the thermal cross-coupling reaction.

▌ Synthesis Design

J. He, K. Bao, W. Cui, J. Yu, C. Huang,*
X. Shen, Z. Cui, N. Wang

■■ – ■■

Construction of Large-Area Uniform Graphdiyne Film for High-Performance Lithium-Ion Batteries